



OPEN

# Mechanism understanding in cryo atomic layer etching of SiO<sub>2</sub> based upon C<sub>4</sub>F<sub>8</sub> physisorption

G. Antoun<sup>1</sup>✉, T. Tillocher<sup>1</sup>, P. Lefaucheux<sup>1</sup>, J. Faguet<sup>2</sup>, K. Maekawa<sup>2</sup> & R. Dussart<sup>1</sup>✉

Cryogenic Atomic Layer Etching (cryo-ALE) of SiO<sub>2</sub> based on alternating a C<sub>4</sub>F<sub>8</sub> molecule physisorption step and an argon plasma step, has been enhanced thanks to a better understanding of the mechanism. First, we used Quadrupole Mass spectrometry (QMS) and spectroscopic ellipsometry analyses to evaluate the residence time of physisorbed C<sub>4</sub>F<sub>8</sub> molecules versus temperature and pressure on SiO<sub>2</sub> surface. QMS monitoring of the SiF<sub>4</sub> etching by-product also enabled to follow the self-limiting etching behavior. Finally, a SiO<sub>2</sub> cryo-ALE process was proposed at a temperature of  $-90^{\circ}\text{C}$  resulting in a very linear etch over 150 cycles and an Etch amount Per Cycle as low as 0.13 nm/cycle.

In the area of nanotechnology and sub-10 nm devices, Atomic Layer Etching (ALE) has become one of the most promising processes to overcome the latest and greatest challenges. More specifically, selective etching of silicon dioxide over other materials such as silicon or silicon nitride have attracted interest from many researchers<sup>1-5</sup>. One of the main solutions to perform anisotropic ALE of SiO<sub>2</sub> is to use fluorocarbon-based plasmas to deposit a very thin FC modified layer on the surface. This layer can then be etched using Ar or O<sub>2</sub> plasma at low ion energy bombardment<sup>2,3,6-11</sup>. However, some drifts were reported in the processes, with an increase of the etch amount per cycle (EPC) due to the fluorine contamination of the reactor walls<sup>8-10,12</sup>. Yet, *Dallorto* et al. have shown that the effect of fluorine from the reactor wall contamination is reduced by decreasing the substrate temperature to  $-10^{\circ}\text{C}$  and below<sup>12</sup>. More generally, cryogenic processes demonstrated to be clean processes with limited chamber wall contamination<sup>13</sup>.

Therefore, cryo-Atomic Layer Etching (Cryo-ALE) is proposed as an alternative to etch SiO<sub>2</sub> in fluorocarbon-based chemistry but without plasma during the deposition step. In this process, the substrate is cooled to a temperature below  $-80^{\circ}\text{C}$ . A C<sub>4</sub>F<sub>8</sub> gas is injected and molecules adsorb on the cooled substrate surface. After purging the gas, an Ar plasma is initiated to activate the etching by low energy ion bombardment. A proof of principle has been previously published<sup>14</sup>, showing that cryo-ALE based on C<sub>4</sub>F<sub>8</sub> physisorption was working at  $-120^{\circ}\text{C}$  in our experimental conditions. However, etching was suppressed at  $-110^{\circ}\text{C}$ , owing to the desorption of C<sub>4</sub>F<sub>8</sub> from the substrate surface being too fast if the temperature is not low enough. Thus, at temperatures below  $-110^{\circ}\text{C}$ , a self-limiting regime was achieved and an etch per cycle as low as 0.4 nm was obtained. With this process, fluorocarbon polymer is no longer deposited on the reactor walls significantly reducing chamber contamination and limiting process drift. As a result, it is easier to control the etching through many etch cycles.

In this article, we report on the residence time of C<sub>4</sub>F<sub>8</sub> versus temperature and pressure. Both ellipsometry and mass spectrometry measurements are used to characterize the adsorption and desorption of C<sub>4</sub>F<sub>8</sub> from the SiO<sub>2</sub> surface. The improved understanding of the C<sub>4</sub>F<sub>8</sub> residence time enabled for a significant extension of the SiO<sub>2</sub> cryo-ALE process temperature range towards higher and more practical temperature.

## Experimental methods

In order to understand the adsorption of C<sub>4</sub>F<sub>8</sub>, 150 mm SiO<sub>2</sub> carrier wafers are used, on which SiO<sub>2</sub> coupons are glued. The SiO<sub>2</sub> coupons are composed of (100) silicon samples with 100 nm thick thermal silicon dioxide layer. A special glue material is spread uniformly on the backside of the sample and is stable at very low temperature. It has a very good thermal conductivity and is easily removed after use.

As the coupons consist of thin films of SiO<sub>2</sub> on silicon, they enable a very accurate fit by ellipsometry at the nanoscale.

<sup>1</sup>GREMI, Orléans University-CNRS, 14 Rue d'Issoudun, BP 6744, 45067 Orléans, France. <sup>2</sup>TEL Technology Center, America, LLC, NanoFab 300 South 255 Fuller Rd., Suite 214, Albany, NY, USA. ✉email: gaelle.antoun@univ-orleans.fr; remi.dussart@univ-orleans.fr

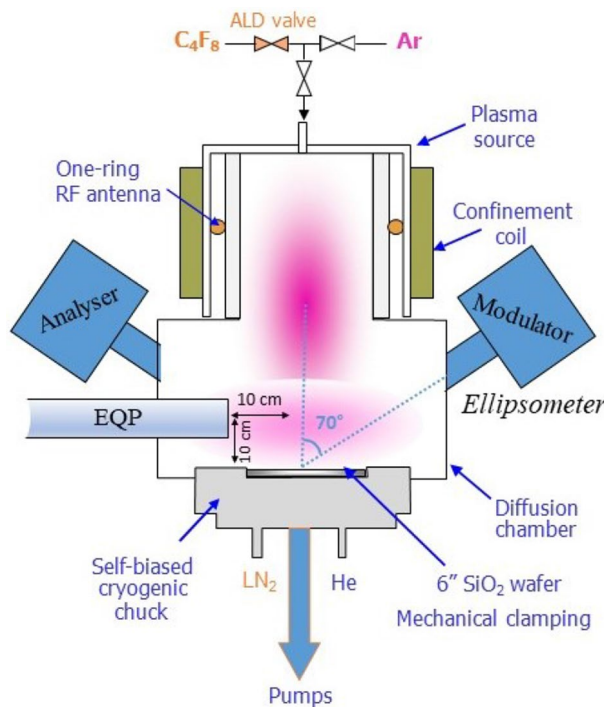


**Figure 1.** Sketch of the cryogenic ICP reactor equipped with QMS and SE.

The prepared samples are then introduced into an inductively coupled plasma reactor that is equipped with a diffusion chamber and a cryogenic substrate holder. The chuck can be cooled down by liquid nitrogen and temperature is controlled and stabilized using a Proportional Integral Derivative (PID) system. Wafers are mechanically clamped and a backside helium pressure provides for an optimal thermal contact with the chuck. A sketch of the reactor can be seen in Fig. 1.

A Horiba Jobin Yvon UVISEL spectroscopic ellipsometer is coupled to the reactor at an incidence angle of 70° to characterize the substrate surface in-situ. It monitors the thickness variation in kinetic mode at the sample surface during the cycles. The sampling interval is set at 2 s, with an integration time of 0.5 s. For each point of acquisition, spectra are acquired using 32 wavelengths from UV to visible. Lorentz and Drude models were then used to model and fit the ellipsometric spectra.

An Electrostatic Quadrupole Mass Spectrometer (QMS) from Hiden Analytical is used in Residual Gas Analysis (RGA) mode to analyze and monitor the species produced or injected in the reactor during the different steps of the ALE cycles. The mass spectrometer can be used in spectrum mode or in Multiple Ion Detection (MID) mode. The electron energy in the ionization chamber is 70 eV. The QMS entrance slit was positioned at 100 mm above the sample and at 100 mm from the center of the reactor.  $\text{C}_4\text{F}_8^+$  mass (100 amu) corresponds to one of the main peaks from the fragmentation spectrum of  $\text{C}_4\text{F}_8$ <sup>15</sup>. Therefore, its signal was acquired to characterize the kinetics of  $\text{C}_4\text{F}_8$  molecules in the chamber. The  $\text{SiF}_3^+$  line intensity at 85 amu was also recorded, during an ALE process, in order to follow the evolution of  $\text{SiF}_4$  molecules in the reactor, especially during the etch step.  $\text{SiF}_3^+$  is reported to be the main fragment ion from  $\text{SiF}_4$ <sup>16</sup>. The intensity of the detected ions is expressed in counts per second (c/s).

## Results

**Atomic layer etching process at low substrate temperature.** In order to characterize and understand the mechanisms involved in Atomic Layer Etching at low substrate temperature, a cryo-ALE process was performed. The generic time chart of cryo-ALE used in<sup>14</sup> is shown as a reminder in Fig. 2.

Figure 3 presents 8 cycles of cryo-ALE monitored by in-situ ellipsometry for the thickness variation and by QMS to follow 85 amu corresponding to  $\text{SiF}_3^+$  signal, which represents  $\text{SiF}_4$ , the main etching by-product. During this process, a  $\text{C}_4\text{F}_8$  gas flow is first injected for 10 s in order to allow for the molecules to physisorb on the cooled substrate surface ( $-120^\circ\text{C}$ ). Then, an Ar purge of 30 s is performed in order to remove  $\text{C}_4\text{F}_8$  molecules from the chamber. After that, the Ar plasma is ignited to activate the etch and sustained for 2 min to ensure self-limiting etching is achieved. Finally, a pumping step is performed before starting the next cycle, in order to evacuate all the etching by-products from the chamber. The physisorption step is clearly identified by ellipsometry measurements, as well as by the QMS signal. The  $\text{SiF}_3^+$  mass of 85 amu is close to the mass of  $\text{C}_4\text{F}_2^+$  (86 amu) which is an ion from the fragmentation of  $\text{C}_4\text{F}_8$ . Hence, as shown in Fig. 3, the first peak of a cycle, observed on QMS signal during the  $\text{C}_4\text{F}_8$  injection is related to  $\text{C}_4\text{F}_2^+$ . When the Ar plasma is initiated, etching is observed by ellipsometry as well as by QMS. During the first three cycles, an increase in  $\text{SiF}_3^+$  signal and the EPC is observed, before it reaches a steady amount. This shows that the first cycles are in transient state.

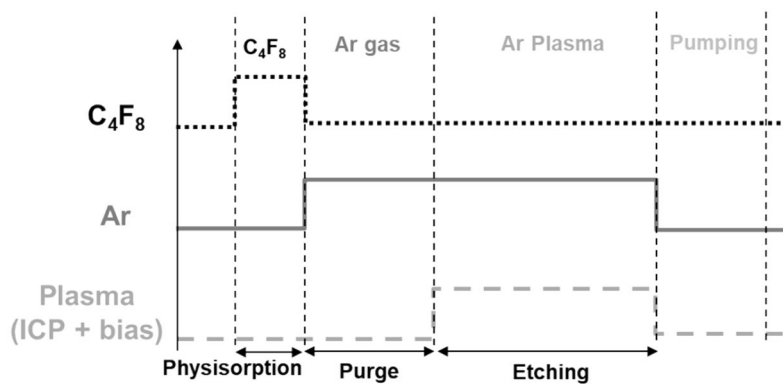


**Figure 2.** Generic time chart of one cryo-ALE cycle.

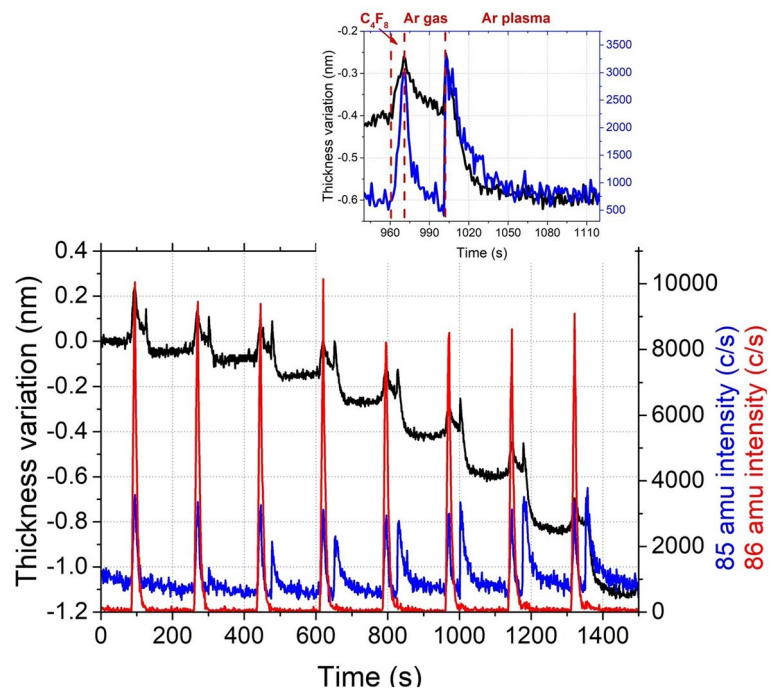


**Figure 3.** Thickness variation measured by ellipsometry and 85 and 86 amu signals by QMS for 8 ALE cycles performed on  $\text{SiO}_2$ , (inset) zoom on the second cycle. (Experimental conditions:  $T = -120\text{ }^\circ\text{C}$ ,  $\text{C}_4\text{F}_8$  flow: 10 s, 1.9 Pa, Ar purge: 30 s, 3.3 Pa, Ar plasma: 2 min, 3.3 Pa,  $P_{\text{source}} = 400\text{ W}$ ,  $V_{\text{bias}} = -20\text{ V}$ , pumping: 15 s, 0 Pa).

Surface contamination may limit the etching during these cycles, as well as the formation of a mixing layer such as  $\text{SiOCF}$  on the surface instead of completion of etching<sup>4,7,17</sup>. Once this layer is formed, the etch amount per cycle becomes constant and self-limiting etching is reached. Then, during the following cycles, the  $\text{SiF}_3^+$  signal steeply increases the first few seconds, and then starts to decrease (see the inset of Fig. 3). This behavior shows that self-limiting etching is almost reached, inducing less etching and less  $\text{SiF}_4$  by-products. The presence of  $\text{SiF}_3^+$  signal clearly indicates that the substrate is etched chemically. Indeed, the presence of the self-limiting etching (SLE) is evidenced from the observation of both the film thickness and the  $\text{SiF}_3^+$  signal simultaneous transition to a plateau, confirming that Ar sputtering does not participate to the etching mechanism. Moreover, the same test, performed at  $-110\text{ }^\circ\text{C}$ , shows no etching, as reported in<sup>14</sup>, as all  $\text{C}_4\text{F}_8$  molecules desorb from the surface before the ignition of the argon plasma.

**Characterization of the physisorption.** *Temperature dependency.* In order to optimize the duration of the argon purge step before plasma initiation, the residence time of the  $\text{C}_4\text{F}_8$  molecules was studied as a function of the setpoint temperature. The  $\text{C}_4\text{F}_8$  gas was injected in the reactor chamber for 1 min at constant pressure (3 Pa) and different temperatures of the  $\text{SiO}_2$  substrate. Then the gas was evacuated during several tens of minutes.

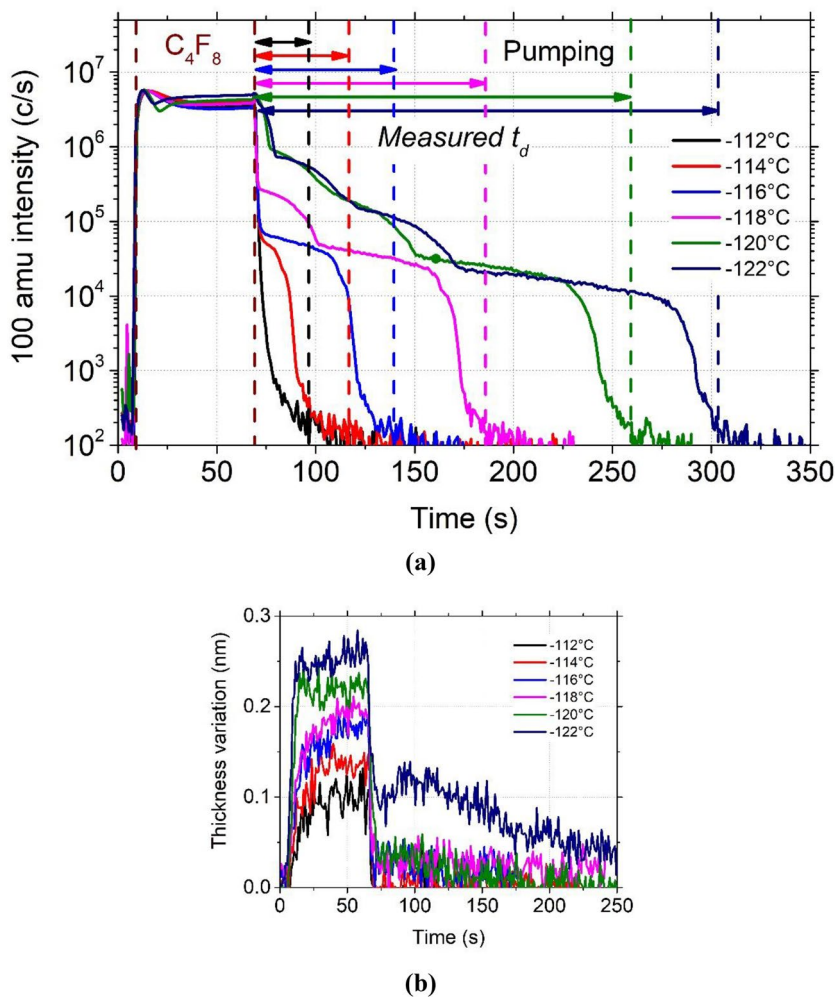


**Figure 4.**  $\text{C}_4\text{F}_8$  physisorption on  $\text{SiO}_2$  depending on setpoint temperature and monitored (a) by QMS by following  $\text{C}_2\text{F}_4^+$  ion peak intensity evolution and (b) by ellipsometry following the thickness variation, both versus time. (Experimental conditions: 1 min  $\text{C}_4\text{F}_8$  flow, 3 Pa followed by a pumping step).

Figure 4a shows the  $\text{C}_2\text{F}_4^+$  line intensity measured by mass spectrometry for various setpoint temperatures between  $-112$  and  $-122$  °C. As soon as  $\text{C}_4\text{F}_8$  gas is injected, the  $\text{C}_2\text{F}_4^+$  signal increases rapidly and stabilizes for a few seconds after injection as the flow is continuously maintained. When the  $\text{C}_4\text{F}_8$  flow is stopped after 1 min of injection, a sharp drop is first observed for all temperatures. Then, different trends are observed depending on the setpoint temperature. At  $-112$  °C, the intensity of  $\text{C}_2\text{F}_4^+$  drops quickly down to a value below  $10^3$  c/s. At  $-114$  °C, the signal drops down to  $8 \times 10^4$  c/s, decreases slowly and drops again after about 20 s. At  $-120$  °C, two different kinetics are observed with two shoulders on the curve: after the  $\text{C}_2\text{F}_4^+$  first drop, a first plateau is reached at  $2 \times 10^4$  c/s, followed by a second decrease and a second plateau. These different drops and plateaus observed in the  $\text{C}_2\text{F}_4^+$  line intensity correspond to different desorption steps of  $\text{C}_4\text{F}_8$ .

To confirm the origin of the first desorption stage,  $\text{C}_4\text{F}_8$  was first physisorbed at  $-120$  °C and then, its desorption was monitored by QMS and ellipsometry. The test was run with and without helium injection between the chuck and the wafer. Without helium, the wafer is not efficiently cooled and nearly no adsorption should occur on it. The results, illustrated in Fig. 5a, show a clear difference between the two cases: the first desorption stage, between 75 and 100 s (indicated in dashed line in Fig. 5a) does not appear when backside helium flow is not used. In Fig. 5b, ellipsometry data confirms that  $\text{C}_4\text{F}_8$  is not adsorbed without helium. With helium, the thickness grows during the adsorption of  $\text{C}_4\text{F}_8$ , then drops when the flow is stopped. However, a small shoulder can be noticed, between 75 and 100 s (indicated in dash line in Fig. 5b), representative of  $\text{C}_4\text{F}_8$  desorption. The difference observed with and without helium shows that the first plateau after the main drop corresponds to the desorption of  $\text{C}_4\text{F}_8$  from the wafer. The other plateaus correspond to desorption of  $\text{C}_4\text{F}_8$  from other parts of the chuck, which are cooled as well but have a slightly lower temperature.

Adsorption kinetics differ from the first adsorption layer to the following ones. Kinetics for the first adsorbed layer and coverage are described by Langmuir theory. Then, each particle in the first layer may be an adsorption center for further adsorbates for the next layers. This multimolecular adsorption kinetic is covered by the BET (Brunauer, Emmett and Teller) theory<sup>17</sup>.

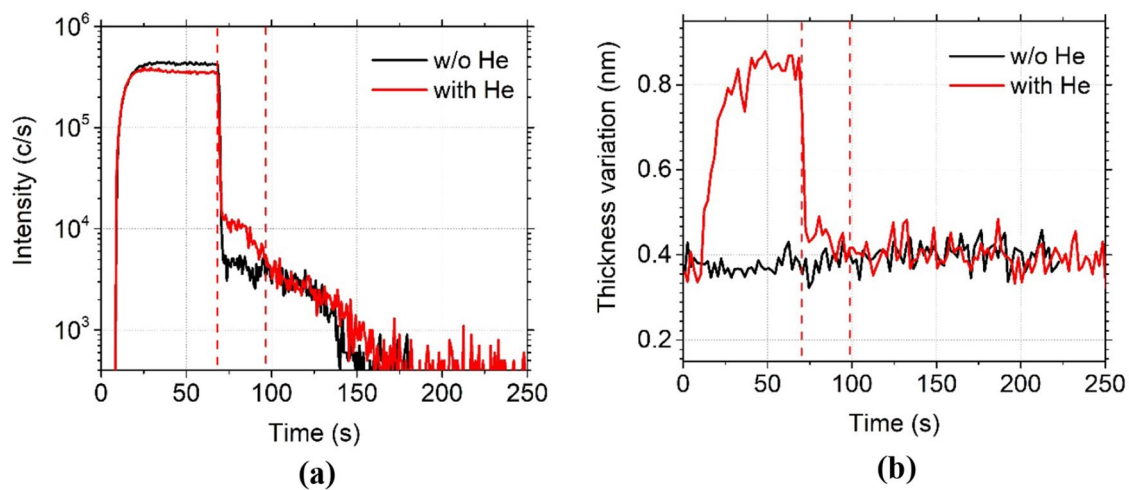


**Figure 5.**  $\text{C}_4\text{F}_8$  physisorption on  $\text{SiO}_2$  depending on the presence of He backside cooling during the clamping and monitored (a) by QMS by following  $\text{C}_2\text{F}_4^+$  ion peak intensity evolution and (b) by ellipsometry following the thickness variation, both versus time. (Experimental conditions:  $T = -120\text{ }^\circ\text{C}$ , 1 min  $\text{C}_4\text{F}_8$  flow, 3 Pa followed by a pumping).

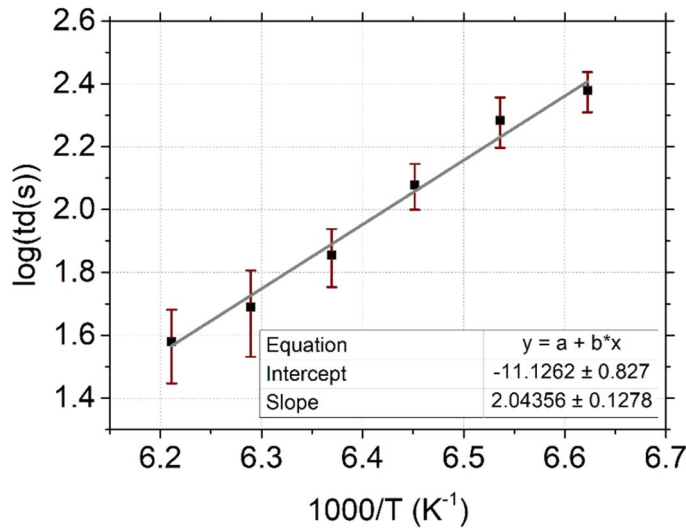


**Figure 6.**  $\text{C}_4\text{F}_8$  desorption rate depending on temperature, for a  $\text{C}_4\text{F}_8$  injection at 3 Pa.

Several layers can adsorb on the wafer surface, and each layer has its specific residence time. The desorption rate decreases with decreasing temperature as the residence time at the surface increases<sup>18</sup>. In the case of those experiments (Fig. 4), according to spectroscopic ellipsometry measurements, the surface coverage is of the order of one or two monolayers at  $-120\text{ }^\circ\text{C}$  and higher temperatures. Consequently, Langmuir model can be applied. For lower temperatures, several layers can adsorb to the surface. However, the desorption rate of top layers is usually much higher than the one of the adsorbed layer on  $\text{SiO}_2$ .

Consequently, from those hypotheses and based on the results obtained by QMS, presented in Fig. 4a, we can consider that the  $\text{C}_4\text{F}_8$  molecules residence time  $t_d$  is the delay between the  $\text{C}_4\text{F}_8$  injection stop and the end of the first slope (Fig. 4a).  $t_d$  was plotted as a function of temperature in Fig. 6. As those measures are extracted from the QMS curves, an error of a few seconds is considered per data point. Then,  $\log(t_d)$  was plotted versus  $1000/T$  and fitted using a linear function. It gave a consistent result with the equation of Frenkel-Arrhenius that enables the determination of surface residence time. The equation being:

$$t_d = t_d^0 \exp^{E_d/k_B T} \quad (1)$$

with  $t_d$  the residence time (s),  $t_d^0$  is the attempt time of the particle for desorption (s),  $E_d$  is the energy to enable the desorption ( $\text{kJ mol}^{-1}$ ),  $k_B$  is the Boltzmann constant ( $\text{kJ K}^{-1}$ ) and  $T$  the substrate temperature (K)<sup>18–20</sup>. From Eq. (1) and the values obtained with the curve fit, the values of  $t_d^0$  and  $E_d$  were determined to be respectively,

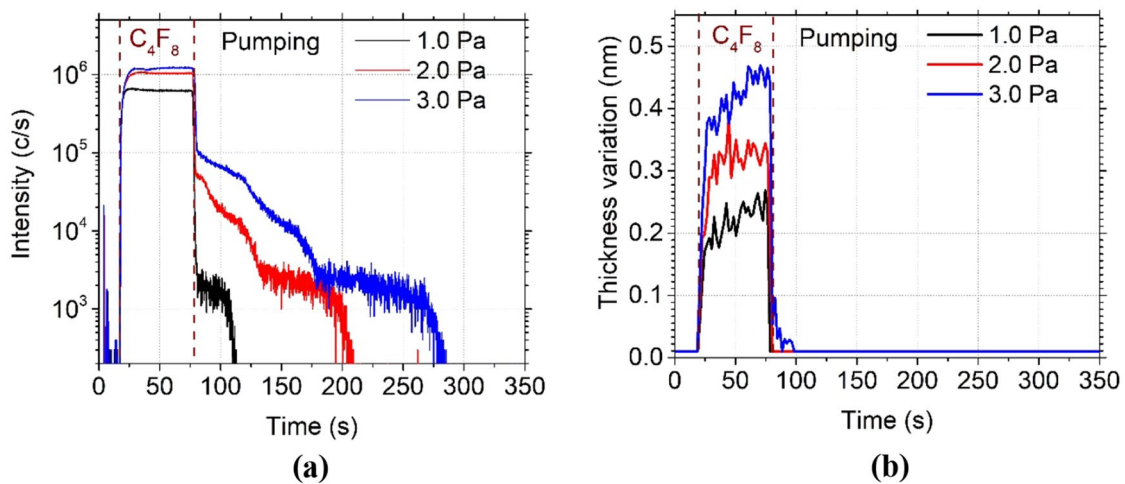


**Figure 7.**  $\text{C}_4\text{F}_8$  physisorption on  $\text{SiO}_2$  depending on pressure and monitored (a) by QMS by following  $\text{C}_2\text{F}_4^+$  ion peak intensity evolution and (b) by ellipsometry following the thickness variation, both versus time. (Experimental conditions:  $T = -120\text{ }^\circ\text{C}$ ,  $\text{C}_4\text{F}_8$  flow: 1 min followed by a pumping).

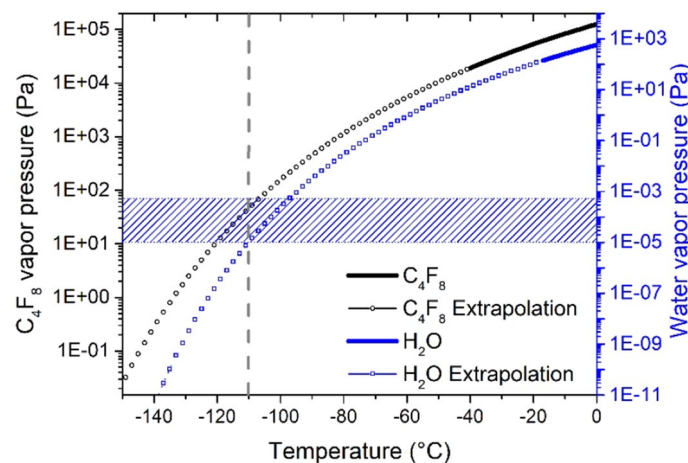


**Figure 8.** Vapor pressure curves for  $\text{H}_2\text{O}$  and  $\text{C}_4\text{F}_8$ .

$1 \times 10^{-11}\text{ s}$  and  $0.406\text{ eV}$  ( $39.1\text{ kJ mol}^{-1}$ ). The desorption energy is very low and is of the order of magnitude of typical binding energy for physisorption.

This graph is of interest to design a cryo-ALE process at different temperatures, especially to define the maximum purge duration between  $\text{C}_4\text{F}_8$  gas injection and the plasma initiation.

**Pressure dependency.** The influence of  $\text{C}_4\text{F}_8$  gas pressure was derived from similar tests obtained by injecting  $\text{C}_4\text{F}_8$  gas for 1 min at different pressures at a temperature set to  $-120\text{ }^\circ\text{C}$ . The results are shown in Fig. 7. Different desorption rates are observed when increasing the pressure. In fact, by increasing the pressure, the density of  $\text{C}_4\text{F}_8$  molecules in the reactor is higher and the quantity of physisorbed molecules is increased. This is also observed by ellipsometry measurements, (Fig. 7b) which show that the thickness of the physisorbed layer increases with pressure. Therefore, it takes a longer time to remove the  $\text{C}_4\text{F}_8$  molecules at a constant desorption rate. Indeed, according to the expression (1) reported in the previous part, the desorption rate does not depend on the gas pressure, but on temperature only.

**Water influence.** For a better understanding of the role of residual water molecules, the vapor pressures curves of  $\text{C}_4\text{F}_8$  and water were plotted together in Fig. 8. In order to cover the temperature range of interest, an extrapolation was performed using Antoine equation parameters from NIST database<sup>21,22</sup>. Hence, in Fig. 8, the part of the curves in bold are from the database and the dotted part lines are extrapolated. The air leakage of the reactor chamber was evaluated at around  $0.1\text{ sccm}$  from which it was possible to estimate the water partial pressure during the  $\text{C}_4\text{F}_8$  gas injection. At  $3\text{ Pa}$ , the water partial pressure is about  $4.3 \times 10^{-4}\text{ Pa}$ , decreasing to  $1.0 \times 10^{-5}\text{ Pa}$  during the pumping. The striped section in Fig. 8 represents the range of water partial pressure in the process

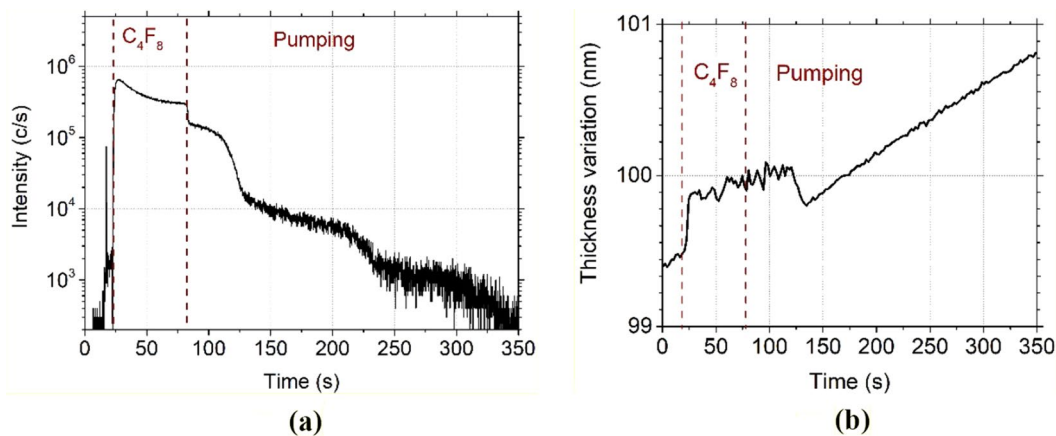


**Figure 9.**  $\text{C}_4\text{F}_8$  physisorption on  $\text{SiO}_2$  at  $-130\text{ }^\circ\text{C}$  monitored (a) by QMS by following  $\text{C}_2\text{F}_4^+$  ion peak intensity evolution and (b) by ellipsometry following the thickness variation, both versus time. (Experimental conditions:  $T = -130\text{ }^\circ\text{C}$ , 1 min  $\text{C}_4\text{F}_8$  flow, 3 Pa followed by a pumping step).

conditions. At temperatures higher than  $-110\text{ }^\circ\text{C}$ , the effect of water is not significant for  $\text{C}_4\text{F}_8$  physisorption, as in these conditions, water does not condensate (on the right of the water curve).

However, for lower temperatures, the parameters are such that water condenses (on the left side of the water curve).

This behavior is observed in Fig. 9 below where physisorption test was performed at  $-130\text{ }^\circ\text{C}$ . During the  $\text{C}_4\text{F}_8$  injection in Fig. 9a the  $\text{C}_2\text{F}_4^+$  signal does not stabilize, but rather decreases although the  $\text{C}_4\text{F}_8$  flow is maintained constant inside the chamber. At this temperature, the cooled substrate acts like a cryogenic pump, and the amount of  $\text{C}_4\text{F}_8$  molecules in the chamber is reduced as they start to condense on the cooled surface of the substrate. This is confirmed by ellipsometry measurements in Fig. 9b: the adsorbed film thickness increases during the  $\text{C}_4\text{F}_8$  injection step instead of reaching a plateau as at higher temperatures (Fig. 4b). This result is consistent with the Antoine's curve giving the vapor pressure of  $\text{C}_4\text{F}_8$  as a function of temperature. By decreasing the temperature, conditions are closer to condensation. Moreover, the point located at  $T = -130\text{ }^\circ\text{C}$  and  $P = 3\text{ Pa}$  is clearly in the condensation part of the water curve. At  $-130\text{ }^\circ\text{C}$ , water molecules, that are present in the chamber, as evidenced by the continuous signal increase after  $\text{C}_4\text{F}_8$  is pumped out, start to condense on the substrate surface. Consequently, it prevents from observing the signal saturation as expected from the  $\text{C}_4\text{F}_8$  physisorption tests in Fig. 4.

**Optimization of the process.** In the letter dedicated to Cryo-ALE<sup>14</sup>, we demonstrated the importance of working at low enough temperature (close to  $-120\text{ }^\circ\text{C}$ ) to reach an etching regime. However, this temperature operating range is often unwanted because it requires the use of liquid nitrogen.

QMS results presented above gave us a better understanding of the mechanisms, enabling the enhancement of the process. The purpose of the following part is to increase the process working temperature.

**Influence of purge step.** According to the physisorption tests results in Fig. 7, when the pressure during the injection of  $\text{C}_4\text{F}_8$  is increased, the amount of  $\text{C}_4\text{F}_8$  molecules that physisorb also increases. Again, this is confirmed in Fig. 10 below, where physisorption tests have been repeated at  $-90\text{ }^\circ\text{C}$  at two different pressures and  $\text{C}_2\text{F}_4^+$  peak was followed by QMS. It shows that at 3.0 Pa,  $\text{C}_2\text{F}_4^+$  signal decreases sharply when  $\text{C}_4\text{F}_8$  is stopped. Whereas, few additional seconds are needed at 6.5 Pa to remove all  $\text{C}_4\text{F}_8$ . By comparing this latter with the test at  $-112\text{ }^\circ\text{C}$  at 3.0 Pa, it is possible to observe that the residence time of  $\text{C}_4\text{F}_8$  at  $-90\text{ }^\circ\text{C}$  6.5 Pa is almost equal to the residence time at  $-112\text{ }^\circ\text{C}$  at 3.0 Pa. This confirms that increasing the pressure will help processing at higher temperatures.

In Figs. 8, 11 cryo-ALE cycles were performed at  $-90\text{ }^\circ\text{C}$ . The pressure of  $\text{C}_4\text{F}_8$  needed to be raised to 6 Pa, which is higher than the usual pressure processing that was used in previous experiments ( $\sim 2\text{--}3\text{ Pa}$ ), to enable the physisorption of few monolayers of  $\text{C}_4\text{F}_8$  molecules. However, the subsequent purge step time is also very critical. If the purge step time is too long, all  $\text{C}_4\text{F}_8$  molecules desorb before starting the argon plasma for the etching step. If it is too short,  $\text{C}_4\text{F}_8$  gas is not totally evacuated from the reactor chamber and  $\text{CF}_x$  are created in the chamber during the Ar plasma. The process may thus no longer be controlled. As observed in Fig. 11, a clear difference is obtained by varying the purge step time by only 1 s. Very low etching is observed at 4 s purge time because most of  $\text{C}_4\text{F}_8$  molecules have desorbed from the surface. Whereas, if the time is decreased to 3 s, a sufficient quantity of molecules is still present at the surface to allow for the etching of 0.3 nm of  $\text{SiO}_2$  per cycle. The Ar plasma in this process lasts only 1 min, which is on the limits for reaching the self-limiting etching plateau. During this etching plasma, half of the etched amount is removed during the first 15 s.

Same test with 3 s for the purge step was performed at  $20\text{ }^\circ\text{C}$ . No etching occurs in this case. This proves that the etching achieved at  $-90\text{ }^\circ\text{C}$  in the same conditions is due to physisorbed species and not from residual  $\text{C}_4\text{F}_8$  in the chamber. It also shows that no sputtering occurs during the Ar plasma.

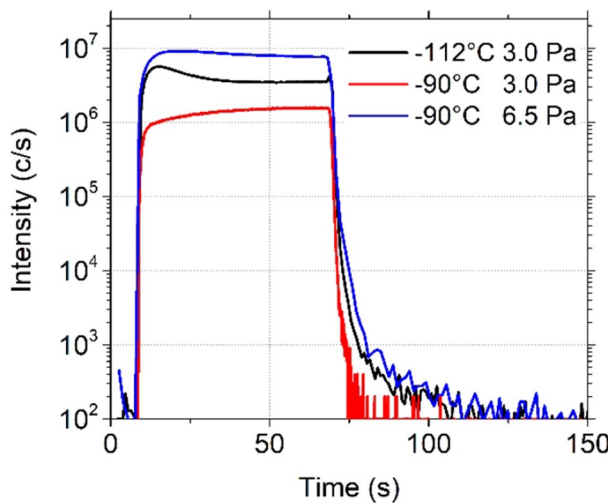


**Figure 10.**  $\text{C}_4\text{F}_8$  physisorption on  $\text{SiO}_2$  depending on pressure and temperature and monitored by QMS by following  $\text{C}_2\text{F}_4^+$  ion peak intensity evolution versus time. (Experimental conditions:  $T = -90\text{ }^\circ\text{C}$  and  $-112\text{ }^\circ\text{C}$ ,  $\text{C}_4\text{F}_8$  flow: 1 min followed by a pumping).

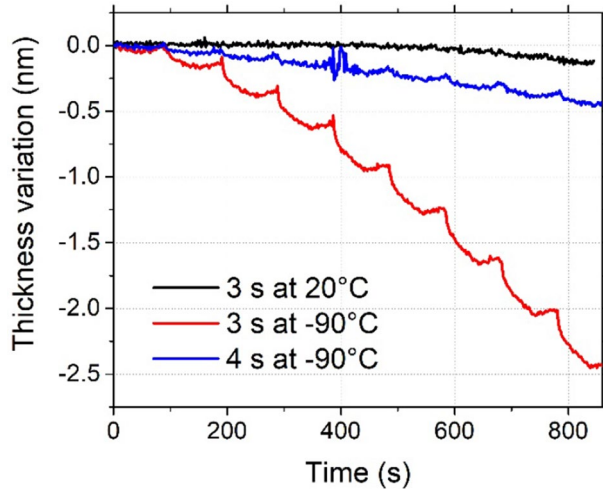


**Figure 11.** 8 ALE cycles performed on  $\text{SiO}_2$  with the thickness variation followed by ellipsometry. (Experimental conditions:  $T = 20\text{ }^\circ\text{C}$  /  $-90\text{ }^\circ\text{C}$ ,  $\text{C}_4\text{F}_8$  flow: 20 s, 6 Pa, Ar purge: 3 s/3 s/4 s,  $< 1\text{ Pa}$ , Ar plasma: 1 min, 3 Pa,  $\text{P}_{\text{source}} = 400\text{ W}$ ,  $\text{V}_{\text{bias}} = -20\text{ V}$ , pumping: 15 s,  $< 1.0 \times 10^{-3}\text{ Pa}$ ).

*Etch cycles repeatability.* It is essential in the nanotechnology industry to be able to run processes without drifts. To check the repeatability and robustness of the process presented in Fig. 11, 150 cryo-ALE cycles have been performed on  $\text{SiO}_2$  at  $-90\text{ }^\circ\text{C}$  and monitored by ellipsometry as shown in Fig. 12a. Relying on observations from Fig. 11, the Ar plasma step time for this process has been reduced to 15 s instead of 1 min, in order to reduce the process time. Figure 12b is an inset showing that it takes about 16 cycles before the process reaches a constant etching amount per cycle. Indeed, during those first cycles, the EPC is first close to  $0.05\text{ nm/cycle}$  and increases until it becomes stable at  $0.13\text{ nm/cycle}$ , until the end of the process (Fig. 12c). The steady etch amount per cycle is in fact reached after having etched  $0.5\text{ nm}$ , which corresponds to approximately one monolayer of  $\text{SiO}_2$ . During those first cycles, the surface is being modified to form a  $\text{SiOCF}$  like layer<sup>4,17</sup>. As the temperature is higher than in the previous processes,  $-90\text{ }^\circ\text{C}$  instead of  $-120\text{ }^\circ\text{C}$ , less  $\text{C}_4\text{F}_8$  is adsorbing per cycle, and consequently, more cycles are needed before reaching a quasi-steady surface state. Once the first monolayer, which is also expected to be contaminated by carbon<sup>7</sup>, is removed, the surface modification remains the same at the beginning of all the cycles: the  $\text{SiO}_2$  layer should contain the same amount of active sites for  $\text{C}_4\text{F}_8$  physisorption. Moreover, the absence of drift supports that processes based on physisorption at low substrate temperature limit reactor wall contamination and hence the occurrence of drifts. The surface roughness remains the same before and after etching and is close to  $0.40\text{ nm}$  for the Root Mean Square roughness ( $\text{R}_q$ ).

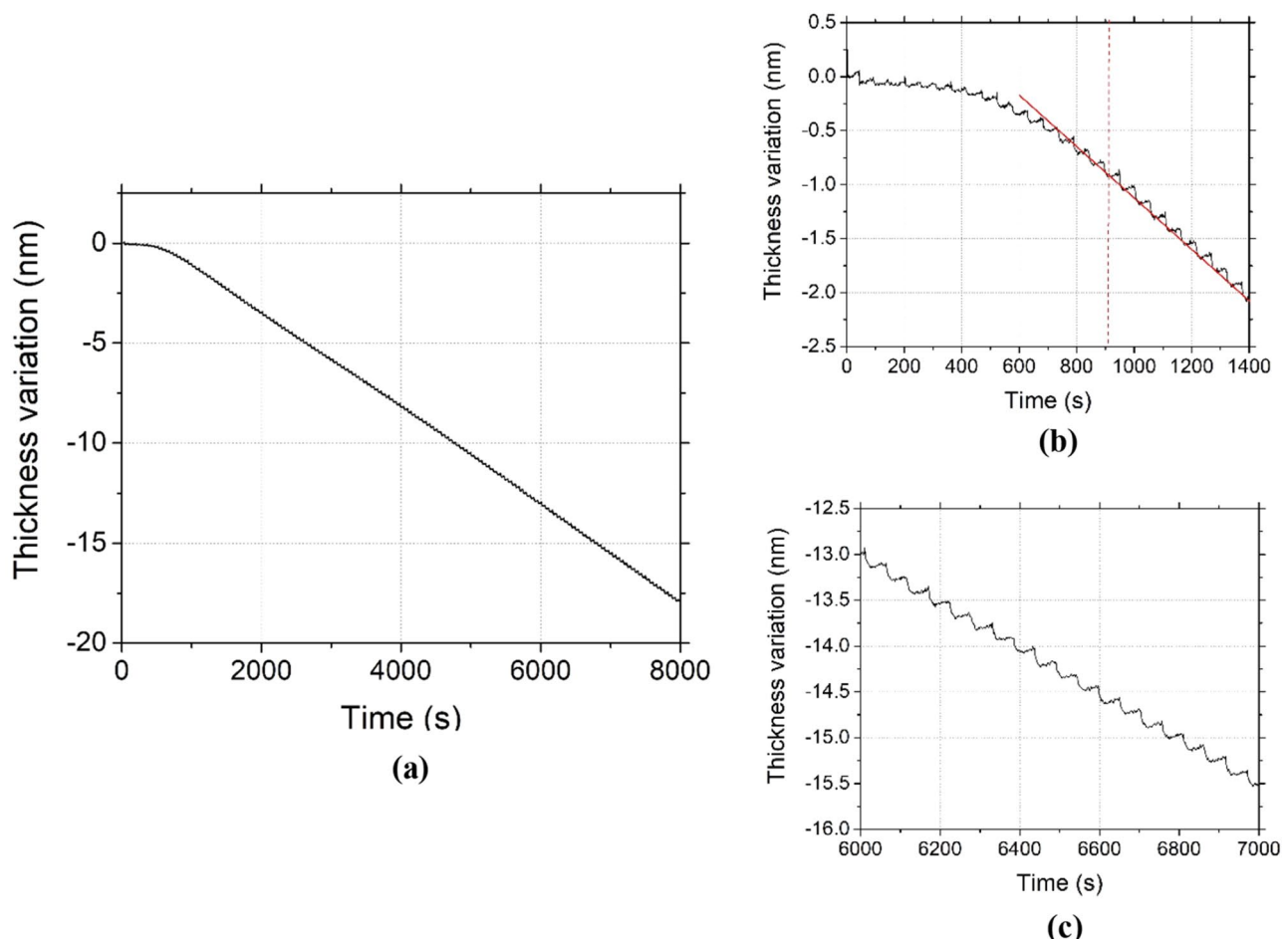


**Figure 12.** (a) 150 ALE cycles performed on  $\text{SiO}_2$ , (b) zoom on the beginning of the process, (c) zoom close to the end of the process. (Experimental conditions:  $T = -90\text{ }^\circ\text{C}$ ,  $\text{C}_4\text{F}_8$  flow: 20 s, 5.5 Pa, Ar purge: 3 s,  $< 1\text{ Pa}$ , Ar plasma: 15 s, 3 Pa,  $\text{P}_{\text{source}} = 400\text{ W}$ ,  $\text{V}_{\text{bias}} = -20\text{ V}$ , pumping: 15 s,  $< 1.0 \times 10^{-3}\text{ Pa}$ ).

## Conclusion

The proposed cryogenic Atomic Layer Etching of  $\text{SiO}_2$  is a process based on a first injection of  $\text{C}_4\text{F}_8$  gas without plasma, followed by argon plasma to activate chemical reactions between physisorbed molecules and  $\text{SiO}_2$  at the surface. QMS and spectroscopic ellipsometry were used to better understand the parameters affecting physisorption and desorption. The increase of residence time of  $\text{C}_4\text{F}_8$  molecules at the surface when decreasing the setpoint temperature was clearly observed by mass spectrometry. At higher pressure, desorption takes more time due to the higher amount of physisorbed molecules. Consequently, the thickness of adsorbed molecules does not reach a plateau as observed at higher temperatures (between  $-90$  and  $-120\text{ }^\circ\text{C}$ ). From these observations, the operating process temperature has been increased from  $-120$  to  $-90\text{ }^\circ\text{C}$ . To this end, the pressure has also been raised from 3 to 6 Pa and the purge step time was decreased to prevent the desorption of all the physisorbed molecules. QMS tests also enabled to monitor the etching and predict reaching of the self-limiting etching by following the  $\text{SiF}_3^+$  signal.

Finally, a remarkably linear etching has been observed when performing 150 cryo-ALE cycles at  $-90\text{ }^\circ\text{C}$ . The absence of a process drift shows, that contamination of the reactor wall remains very low in these cryogenic process conditions.

Received: 15 September 2020; Accepted: 8 December 2020

Published online: 11 January 2021

## References

1. Gasvoda, R. J., Verstappen, Y. G. P., Wang, S., Hudson, E. A. & Agarwal, S. Surface prefunctionalization of  $\text{SiO}_2$  to modify the etch per cycle during plasma-assisted atomic layer etching. *J. Vac. Sci. Technol. A* **37**, 051003 (2019).
2. Wang, M., Ventzek, P. L. G. & Ranjan, A. Quasiamolecular layer etching of silicon oxide selective to silicon nitride in topographic structures using fluorocarbon plasmas. *J. Vac. Sci. Technol. Vac. Surf. Films* **35**, 031301 (2017).
3. Li, C., Metzler, D., Lai, C. S., Hudson, E. A. & Oehrlein, G. S. Fluorocarbon based atomic layer etching of  $\text{Si}_3\text{N}_4$  and etching selectivity of  $\text{SiO}_2$  over  $\text{Si}_3\text{N}_4$ . *J. Vac. Sci. Technol. Vac. Surf. Films* **34**, 041307 (2016).
4. Metzler, D. *et al.* Characterizing fluorocarbon assisted atomic layer etching of Si using cyclic Ar/C4F8 and Ar/CHF3 plasma. *J. Chem. Phys.* **146**, 052801 (2017).

5. Lin, K.-Y. *et al.* Achieving ultrahigh etching selectivity of SiO<sub>2</sub> over Si<sub>3</sub>N<sub>4</sub> and Si in atomic layer etching by exploiting chemistry of complex hydrofluorocarbon precursors. *J. Vac. Sci. Technol. A* **36**, 040601 (2018).
6. Metzler, D., Bruce, R. L., Engelmann, S., Joseph, E. A. & Oehrlein, G. S. Fluorocarbon assisted atomic layer etching of SiO<sub>2</sub> using cyclic Ar/C<sub>4</sub>F<sub>8</sub> plasma. *J. Vac. Sci. Technol. Vac. Surf. Films* **32**, 020603 (2014).
7. Kaler, S. S., Lou, Q., Donnelly, V. M. & Economou, D. J. Atomic layer etching of silicon dioxide using alternating C<sub>4</sub>F<sub>8</sub> and energetic Ar<sup>+</sup> plasma beams. *J. Phys. Appl. Phys.* **50**, 234001 (2017).
8. Kawakami, M., Metzler, D., Li, C. & Oehrlein, G. S. Effect of the chamber wall on fluorocarbon-assisted atomic layer etching of SiO<sub>2</sub> using cyclic Ar/C<sub>4</sub>F<sub>8</sub> plasma. *J. Vac. Sci. Technol. Vac. Surf. Films* **34**, 040603 (2016).
9. Gasvoda, R. J., van de Steeg, A. W., Bhowmick, R., Hudson, E. A. & Agarwal, S. Surface phenomena during plasma-assisted atomic layer etching of SiO<sub>2</sub>. *ACS Appl. Mater. Interfaces* **9**, 31067–31075 (2017).
10. Tsutsumi, T. *et al.* Atomic layer etching of SiO<sub>2</sub> by alternating an O<sub>2</sub> plasma with fluorocarbon film deposition. *J. Vac. Sci. Technol. Vac. Surf. Films* **35**, 01A103 (2017).
11. Dallorto, S. *et al.* Balancing ion parameters and fluorocarbon chemical reactants for SiO<sub>2</sub> pattern transfer control using fluorocarbon-based atomic layer etching. *J. Vac. Sci. Technol. B* **37**, 051805 (2019).
12. Dallorto, S. *et al.* Atomic layer etching of SiO<sub>2</sub> with Ar and CHF<sub>3</sub> plasmas: a self-limiting process for aspect ratio independent etching. *Plasma Process. Polym.* **16**, 1900051 (2019).
13. Dussart, R., Tillocher, T., Lefaucheux, P. & Boufnichel, M. Plasma cryogenic etching of silicon: from the early days to today's advanced technologies. *J. Phys. Appl. Phys.* **47**, 123001 (2014).
14. Antoun, G. *et al.* Cryo atomic layer etching of SiO<sub>2</sub> by C<sub>4</sub>F<sub>8</sub> physisorption followed by Ar plasma. *Appl. Phys. Lett.* **115**, 153109 (2019).
15. Li, X. *et al.* Properties of C4F8 inductively coupled plasmas. I. Studies of Ar/C4F8 magnetically confined plasmas for etching of SiO<sub>2</sub>. *J. Vac. Sci. Technol. A* **22**, 11 (2004).
16. Basner, R., Schmidt, M., Denisov, E., Becker, K. & Deutsch, H. Absolute total and partial cross sections for the electron impact ionization of tetrafluorosilane (SiF<sub>4</sub>). *J. Chem. Phys.* **114**, 1170–1177 (2001).
17. Kanarik, K. J. *et al.* Predicting synergy in atomic layer etching. *J. Vac. Sci. Technol. Vac. Surf. Films* **35**, 05C302 (2017).
18. Brunauer, S., Emmett, P. H. & Teller, E. Adsorption of gases in multimolecular layers. *J. Am. Chem. Soc.* **60**, 309–319 (1938).
19. Kreuzer, H. J. & Gortel, Z. W. *Physisorption Kinetics* Vol. 1 (Springer, Berlin Heidelberg, 1986).
20. Tinck, S., Neyts, E. C. & Bogaerts, A. Fluorine-silicon surface reactions during cryogenic and near room temperature etching. *J. Phys. Chem. C* **118**, 30315–30324 (2014).
21. Unnikrishnan, P. & Srinivas, D. Chapter 3—Heterogeneous Catalysis. In *Industrial Catalytic Processes for Fine and Specialty Chemicals* (eds Joshi, S. S. & Ranade, V. V.) 41–111 (Elsevier, Amsterdam, 2012). <https://doi.org/10.1016/B978-0-12-801457-8.00003-3>.
22. Kletskii, A. B. & Petric, L. E. Dependence of vapor pressure of perfluorocyclobutane. *Zh. Fiz. Khim.* **41**, 1183–1184 (1967).
23. Stull, D. R. Vapor pressure of pure substances. organic and inorganic compounds. *Ind. Eng. Chem.* **39**, 517–540 (1947).

## Acknowledgements

The authors gratefully thank Shigeru Tahara from TEL for all the helpful discussions and also Kumiko Yamazaki and Nagisa Sato from TEL for their support to the project.

This work was supported by the CERTeM 2020 platform, which provides most of the equipment.

## Author contributions

G.A., T.T., R.D. wrote the main manuscript text. P.L., J.F. and K.M. helped with the results discussions and choice of figures. All authors reviewed the manuscript.

## Competing interests

The authors declare no competing interests.

## Additional information

**Correspondence** and requests for materials should be addressed to G.A. or R.D.

**Reprints and permissions information** is available at [www.nature.com/reprints](http://www.nature.com/reprints).

**Publisher's note** Springer Nature remains neutral with regard to jurisdictional claims in published maps and institutional affiliations.



**Open Access** This article is licensed under a Creative Commons Attribution 4.0 International License, which permits use, sharing, adaptation, distribution and reproduction in any medium or format, as long as you give appropriate credit to the original author(s) and the source, provide a link to the Creative Commons licence, and indicate if changes were made. The images or other third party material in this article are included in the article's Creative Commons licence, unless indicated otherwise in a credit line to the material. If material is not included in the article's Creative Commons licence and your intended use is not permitted by statutory regulation or exceeds the permitted use, you will need to obtain permission directly from the copyright holder. To view a copy of this licence, visit <http://creativecommons.org/licenses/by/4.0/>.

© The Author(s) 2021, corrected publication 2022